

Branch Companion Modeling for Diverse Simulation of Electromagnetic and Electromechanical Transients

Rachel Shintaku, Kai Strunz

Abstract—Simulators of the Electromagnetic Transients Program (EMTP) type are widely used for the study of high-frequency transients in power electric systems. For the study of electromechanical transients, where the main interest is to focus only on deviations from the AC waveform, the EMTP approach is not efficient. In this paper, a branch companion model that is suitable for both electromagnetic and electromechanical transients simulation is proposed. It processes analytic signals whose Fourier spectrum can be shifted in accordance with the objective of the study. The proposed method opens the way for a unified description of electromagnetic and electromechanical transients simulation.

Index Terms—Algorithms, electromagnetic transients, electromechanical transients, modeling, power system simulation, power system transients.

I. INTRODUCTION

Simulators derived from the Electromagnetic Transients Program EMTP [1] are the most widely used tools for the emulation of electromagnetic transients in power systems. In the EMTP, the differential equations describing the behavior of the branches of the network are discretized using trapezoidal integration. The resulting difference equations are rearranged so that each branch is modeled through a circuit consisting of resistors and DC sources, and this branch model is also known as a companion model [2]. The network model is obtained by connecting the companion models in accordance with the topology of the network of interest. Mathematically, this step is implemented using nodal analysis techniques and the stamping method for direct construction of the nodal admittance matrix of the network. The effectiveness of this approach has contributed to the popularity of the EMTP.

For the study of electromechanical transients, the EMTP approach is not efficient. Electromechanical transients entail low-frequency deviations from the carrier frequency, which is either 50 Hz or 60 Hz in large power electric systems. In the

EMTP simulation, the carrier frequency component as well as deviations are represented. Therefore, the time step must be chosen sufficiently small to allow for the representation of the carrier frequency component.

Since it is often desirable to study only the electromechanical transients, simulators based on phasor calculus that eliminate the carrier frequency component from the waveforms were developed. Dynamic phasors are defined as the complex time-varying Fourier series coefficients associated with the waveforms [3]–[5]. In [6], dynamic phasor calculus was combined with time step control and has been shown to cover a spectrum ranging from electromechanical to electromagnetic transients.

The contribution of this work lies in the creation of a branch companion model that can be used both for power system simulation of the EMTP type as for simulation of the dynamic phasor type. Following this introduction, the EMTP type is reviewed in Section II. In Section III, the novel method is discussed. An application example is studied in Section IV. Conclusions are drawn and an outlook is given in Section V.

II. ELECTROMAGNETIC TRANSIENTS SIMULATION

In what follows, three concepts essential to EMTP simulation are reviewed: the discretization of the differential equations, companion modeling, and network modeling.

A. Discretization

The behavior of the inductor depicted in Fig. 1 is described through the following differential equation:

$$\frac{di_L(t)}{dt} = \frac{v_L(t)}{L}. \quad (1)$$

Trapezoidal integration [7] yields:

$$\frac{i_L(k) - i_L(k-1)}{\tau} = \frac{v_L(k) + v_L(k-1)}{2L}, \quad (2)$$

where k is the time step counter, and τ is the time step size.

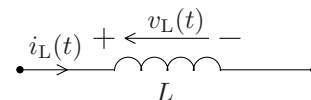


Fig. 1. Current and voltage conventions for an inductor

The authors gratefully acknowledge support from the National Science Foundation under award ECS-0238523 and Sandia National Laboratories through contract 184630.

R. Shintaku is with Boeing Commercial Airplanes, Seattle, USA.
K. Strunz is with the SESAME Laboratory, Department of Electrical Engineering, University of Washington, Seattle, USA.
Web: www.ee.washington.edu/research/sesame.

B. Companion Modeling

The discretized form (2) can be rearranged as follows:

$$i_L(k) = G_L v_L(k) + \eta_L(k), \quad (3)$$

with:

$$G_L = \frac{\tau}{2L}, \quad (4)$$

$$\eta_L(k) = i_L(k-1) + \frac{\tau}{2L} v_L(k-1). \quad (5)$$

The inductor is thus modeled through a conductance G_L and a history source $\eta_L(k)$. The resulting companion model is shown in Fig. 2.

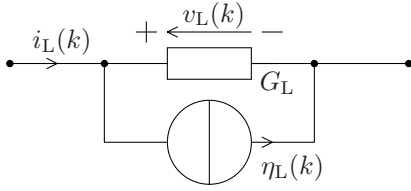


Fig. 2. Companion model of an inductor for electromagnetic transients simulation

In the same way as for the inductor, models can be found for other branches of networks and circuits [1]. In the case of nonlinear branches, the equivalent conductance may change during simulation.

C. Network Modeling

The network model is obtained through direct construction [2], also referred to as stamping, where all branches are conceptually removed from the network and then added successively in order to add the contributions of the companion model conductances to the emerging nodal admittance matrix in accordance with the network topology. The equation system for the network model is then of the following form:

$$\mathbf{Y}(k)\mathbf{v}(k) = \mathbf{j}(k). \quad (6)$$

If there are N unknown nodal voltages, then the nodal admittance matrix \mathbf{Y} is of size $N \times N$. Vector \mathbf{v} contains the unknown and dependent nodal voltages, and \mathbf{j} is the vector of the source dependent nodal current injections. It is assumed that the vector \mathbf{j} is known as it contains contributions from history sources and excitation functions. The equation system is solved at each time step k for \mathbf{v} .

III. DIVERSE ELECTROMAGNETIC AND ELECTROMECHANICAL TRANSIENTS SIMULATION

Electromechanical transients entail waveforms of narrow bandwidth and, as discussed in Section III-A, these waveforms can therefore be represented as equivalent lowpass signals in the form of complex envelopes. In Section III-B, the difference term resulting from the discretization of the differential equation is applied to the complex envelope rather than the

original real signal. Because of the lowpass character and lower maximum frequency, a larger sampling rate can be used to accurately track the transformed signals. In Section III-C, the difference equation is brought into a format that allows for the representation in the form of a companion model. The latter can be used for electromagnetic and electromechanical transients simulation. In Section III-D, the setting of a novel simulation parameter is considered. The network modeling is discussed in Section III-E.

A. Complex Envelope

The complex envelope $\mathcal{E}[\underline{s}(t)]$ of a real bandpass signal $s(t)$ with a carrier frequency f_c is obtained through two major steps. First, the so-called analytic signal $\underline{s}(t)$ [8] is formed by adding to $s(t)$ an imaginary part that is equal to the Hilbert transform of $s(t)$. Second, the Fourier spectrum $\mathcal{F}[\underline{s}(t)]$ is shifted by f_c towards lower frequencies.

1) *Hilbert Transform*: The Hilbert transform is defined as follows:

$$\mathcal{H}[s(t)] = \frac{1}{\pi} \int_{-\infty}^{\infty} \frac{s(\rho)}{t-\rho} d\rho. \quad (7)$$

Once $\mathcal{H}[s(t)]$ is known, the analytic signal can be formed by adding $\mathcal{H}[s(t)]$ as a quadrature component:

$$\underline{s}(t) = s(t) + j\mathcal{H}[s(t)]. \quad (8)$$

The effect of the creation of the analytic signal on the Fourier spectrum of a bandpass signal is shown in Fig. 3. While the spectrum of the real signal $s(t)$ extends to negative frequencies, this is not the case for the spectrum of the corresponding analytic signal $\underline{s}(t)$.

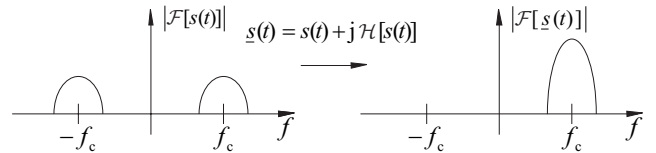


Fig. 3. Application of the Hilbert transform

2) *Frequency Shifting*: The analytic signal can be shifted by the frequency f_s , which is hereafter referred to as shift frequency, as follows:

$$\mathcal{S}[\underline{s}(t)] = \underline{s}(t) e^{-j2\pi f_s t}. \quad (9)$$

For $f_s = f_c$, the complex envelope is obtained:

$$\mathcal{E}[\underline{s}(t)] = \underline{s}(t) e^{-j2\pi f_c t}. \quad (10)$$

Through this operation, the spectrum is shifted by the carrier frequency f_c as shown in Fig. 4.

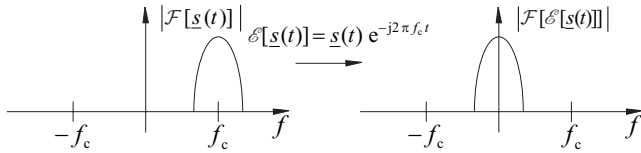


Fig. 4. Shifting by the carrier frequency

The angular shift frequency is directly related to the shift frequency:

$$\omega_s = 2\pi f_s. \quad (11)$$

B. Discretization

As also suggested in [5], the waveforms can be represented through analytic signals in order to exploit the concept of complex envelopes in the context of simulation. Using analytic signals, (1) becomes:

$$\frac{d\underline{i}_L(t)}{dt} = \frac{\underline{v}_L(t)}{L}. \quad (12)$$

The corresponding shifted analytic signals are obtained as follows:

$$\mathcal{S}[\underline{i}_L(t)] = \underline{i}_L(t) e^{-j\omega_s t}. \quad (13)$$

Insertion into (12) yields:

$$\frac{d(\mathcal{S}[\underline{i}_L(t)] e^{j\omega_s t})}{dt} = \frac{\underline{v}_L(t)}{L}. \quad (14)$$

Eq. (14) can be expanded as follows:

$$\frac{d\mathcal{S}[\underline{i}_L(t)]}{dt} e^{j\omega_s t} + j\omega_s \underline{i}_L(t) = \frac{\underline{v}_L(t)}{L}, \quad (15)$$

and solved for the derivative:

$$\frac{d\mathcal{S}[\underline{i}_L(t)]}{dt} = e^{-j\omega_s t} \left(-j\omega_s \underline{i}_L(t) + \frac{\underline{v}_L(t)}{L} \right). \quad (16)$$

Trapezoidal integration is used to transform (16) into a difference equation:

$$\frac{\mathcal{S}[\underline{i}_L(k)] - \mathcal{S}[\underline{i}_L(k-1)]}{\tau} = \frac{e^{-j\omega_s k\tau}}{2} \times \left(-j\omega_s (\underline{i}_L(k) + \underline{i}_L(k-1)) e^{j\omega_s \tau} + \frac{\underline{v}_L(k) + \underline{v}_L(k-1)}{L} e^{j\omega_s \tau} \right). \quad (17)$$

The difference term on the left of (17) is expressed in terms of the complex shifted waveform. For $f_s = f_c$, the complex shifted waveform equals the complex envelope. Its Fourier spectrum has a lower maximum frequency compared with the Fourier spectrum of the analytic signal. Consequently, a larger time step size can be used to track the waveform in simulation. This in turn leads to a smaller computational effort.

C. Branch Modeling

Backsubstitution of complex variables and the gathering of like terms in (17) yields:

$$\frac{\underline{i}_L(k) - \underline{i}_L(k-1) e^{j\omega_s \tau}}{\tau} = \frac{1}{2} \left(-j\omega_s (\underline{i}_L(k) + \underline{i}_L(k-1)) e^{j\omega_s \tau} + \frac{\underline{v}_L(k) + \underline{v}_L(k-1) e^{j\omega_s \tau}}{L} \right). \quad (18)$$

Eq. (18) can be rearranged as follows:

$$\underline{i}_L(k) = \underline{G}_L \underline{v}_L(k) + \underline{\eta}_L(k), \quad (19)$$

with:

$$\underline{G}_L = \frac{\tau}{2L(1 + j\omega_s \frac{\tau}{2})}, \quad (20)$$

$$\underline{\eta}_L(k) = e^{j\omega_s \tau} \left(\frac{1 - j\omega_s \frac{\tau}{2}}{1 + j\omega_s \frac{\tau}{2}} \underline{i}_L(k-1) + \frac{\tau}{2L(1 + j\omega_s \frac{\tau}{2})} \underline{v}_L(k-1) \right). \quad (21)$$

This is the same format as found for Eqs. (3), (4), and (5). Therefore, the companion model is of the same structure as shown in Fig. 5. It differs from the one in Fig. 2 in that now complex quantities appear.

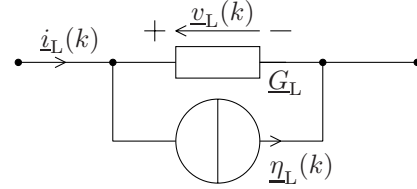


Fig. 5. Companion model of an inductor for diverse electromagnetic and electromechanical transients simulation

The envelopes of the waveforms can be represented very efficiently for $f_s = f_c$. For $f_s = 0$ Hz, \underline{G}_L in (4) and $\underline{\eta}_L$ in (5) can be derived from \underline{G}_L in (20) and $\underline{\eta}_L$ in (21) and are therefore suitable for representing the carrier. Models for branches other than the inductor are derived in an analogous manner.

D. Shift Frequency Setting

The shift frequency is an additional simulation parameter that has been introduced here. It is set prior to the simulation start depending on the type of phenomena to be studied. For the simulation of electromagnetic transients, no frequency shifting is required. However, if the simulation of electromechanical transients is considered, then $f_s = f_c$ is appropriate.

E. Network Modeling

Nodal analysis techniques are used in the same way as described in Section II-C. The companion models for diverse

electromagnetic and electromechanical transients simulation are used. This leads to a complex form of (6):

$$\underline{\mathbf{Y}}(k)\underline{\mathbf{v}}(k) = \underline{\mathbf{j}}(k). \quad (22)$$

The meaning of the symbols corresponds to those introduced for Eq. (6).

IV. APPLICATION

In order to test the method, it is implemented as simulator VISTA (Virtual Integration for Synthesis, Testing and Analysis). The network in Fig. 6 is considered as a test case. A three-phase AC source is connected to an infinite bus via a step-up transformer and a short line. The AC source is representative of a 60 Hz distributed synchronous generating unit with a rating of 50 kVA, 480 V. The reactances are given in per unit on the base of 50 kVA, 480 V. The assumed balanced conditions allow for per-phase analysis [9], performed hereafter. The infinite bus serves as the reference to measure angles: $\underline{E}_\infty = 0.98 \angle 0^\circ$. The steady state conditions are marked by subscript 0:

$$\begin{aligned} \underline{E}_0 &= 1.10 \angle 24.7^\circ, & \underline{V}_0 &= 1.00 \angle 10.7^\circ, \\ \underline{I}_0 &= 0.92 \angle -2.4^\circ, & P_0 &= 0.9. \end{aligned}$$

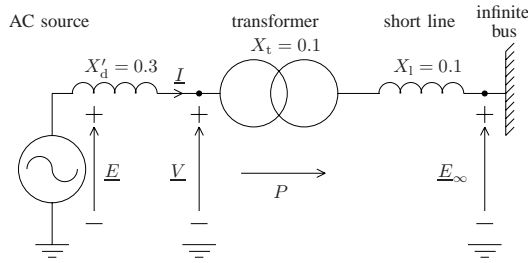


Fig. 6. Test network for AC source perturbation in a balanced three-phase network represented for per-phase analysis.

Assuming that the generator has the small inertia constant of $H = 1.5$ s and that the overall system is lossless, the natural frequency of the system at which undamped electromechanical oscillations occur is $f_n = 2.5$ Hz [10]. This means that small perturbations of the angle of the AC source describe undamped harmonic oscillations at the natural frequency.

In the performed test simulations, the amplitude of the oscillation described by the angle of the AC source was $\hat{\delta}_E = 3^\circ$. Two different time step sizes were considered. In the first case, the time step size of $50 \mu\text{s}$ was used and the frequency shift was $f_s = 0$ Hz. This is an appropriate setting for an electromagnetic transients simulation. The AC waveform of the terminal current $i(t)$, which corresponds to \underline{I} in Fig. 6, and the extracted envelope are shown in Fig. 7.

This is a type of simulation where the envelope information is of strong interest, as is typical of an electromechanical transients simulation. For tracking the envelope, a much larger time step size can be chosen when $f_s = 60$ Hz. In Fig. 8 this is illustrated for $\tau = 5$ ms, $f_s = 60$ Hz. Since the time step size was increased by a factor of 100 compared with the case when $f_s = 0$ Hz, the computational effort was reduced very strongly.

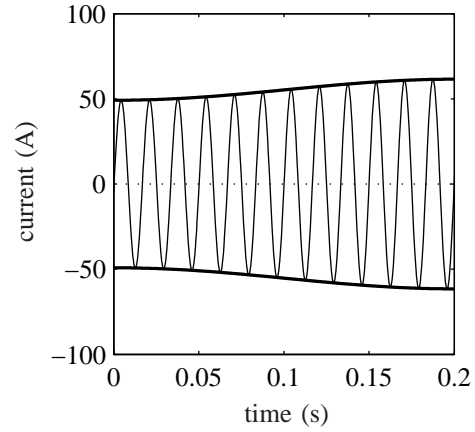


Fig. 7. Carrier and envelope of terminal current $i(t)$ simulated at $f_s = 0$ Hz with $\tau = 50 \mu\text{s}$; solid light: carrier; solid bold: envelope.

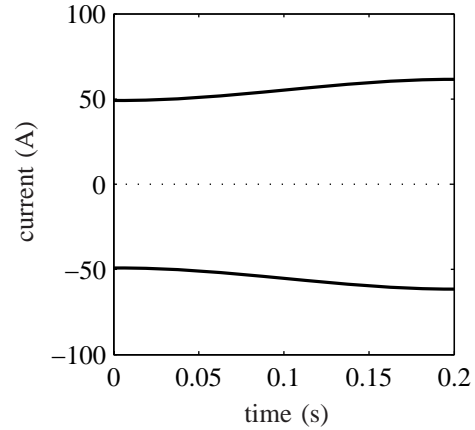


Fig. 8. Envelope of terminal current $i(t)$ simulated at $f_s = 60$ Hz with $\tau = 5$ ms.

V. CONCLUSIONS AND OUTLOOK

A concept for the modeling of network branches for the diverse simulation of electromagnetic and electromechanical transients simulation was introduced. It allows a unified description of branch characteristics and efficient simulation of diverse transients. The developed branch companion model processes analytic signals and contains the shift frequency as a parameter. For $f_s = 0$ Hz, the Fourier spectrum is retained as it is in the case of simulators of the EMTP type used for electromagnetic transients simulation. For $f_s = 60$ Hz, the simulation is based on dynamic phasors of interest for electromechanical transients simulation. The network model is constructed using the stamping method.

With the enhanced capability, the complexity is also increased. An important direction of further work is therefore aimed at facilitating the application of the proposed methodology. For example, the setting of the shift frequency f_s can be automated. To do so, the simulated signals are checked for the presence of a carrier and the shift frequency can be set accordingly. In this context, it is also possible to consider diverse shift frequency settings within one simulation. The integrated simulation of electromagnetic and electromechanical transients based on one methodology can so be coupled with ease of use.

REFERENCES

- [1] H. W. Dommel. Digital computer solution of electromagnetic transients in single- and multiphase networks. *IEEE Transactions on Power Apparatus and Systems*, PAS-88(4):388–399, April 1969.
- [2] L. O. Chua and P.-M. Lin. *Computer Aided Analysis of Electronic Circuits: Algorithms and Computational Techniques*. Prentice-Hall, Englewood Cliffs, N. J., 1975.
- [3] D. Maksimović, A. Stanković, V. Thottuvelil, and G. Verghese. Modeling and simulation of power electronic converters. *Proceedings of the IEEE*, 89(6):898–912, June 2001.
- [4] V. Venkatasubramanian. Tools for dynamic analysis of the general large power system using time-varying phasors. *International Journal of Electrical Power & Energy Systems*, 16(6):365–376, December 1994.
- [5] S. Henschel, A. I. Ibrahim, and H. W. Dommel. Applications of a new EMTP line model for short overhead lines and cables. *International Journal of Electrical Power & Energy Systems*, 21(3):191–198, March 1999.
- [6] S. Henschel, D. Lindenmeyer, T. Niimura, and H. W. Dommel. Intelligent step size control for fast time-domain power system simulation. In *Thirteenth Power System Computation Conference (PSCC)*, pages 1139–1145, Trondheim, Norway, June 1999.
- [7] R. W. Hamming. *Numerical methods for scientists and engineers*. McGraw-Hill, New York, USA, 1962.
- [8] H. D. Lüke. *Signalübertragung*. Springer-Verlag, Berlin, fourth edition, 1990.
- [9] A. R. Bergen and V. Vittal. *Power Systems Analysis*. Prentice-Hall, Upper Saddle River, USA, second edition, 2000.
- [10] P. Kundur. *Power System Stability and Control*. McGraw-Hill, New York, 1993.



Rachel Shintaku graduated with the B. S. degree in electrical engineering from the University of Washington in 2004. Upon graduation, she joined Boeing in Seattle. In 2003, she researched energy system simulation methods and was awarded the Electric Energy Industrial Consortium Assistantship. She received the Grainger Scholarship in 2004.



Dr. Kai Strunz graduated with the Dipl.-Ing. degree from the University of Saarland in Saarbrücken, Germany, in 1996, and he was awarded the Dr.-Ing. degree with summa cum laude from the same university in 2001. From 1995 to 1997, Dr. Strunz pursued research at Brunel University in London. From 1997 to 2002, he worked at the Division Recherche et Développement of Electricité de France (EDF) in the Paris area. In April 2002, he joined the University of Washington as an assistant professor. He is the Convener of CIGRE Task Force C6.04.02 on computational tools for the study of distributed energy resources.

Kai Strunz received the Dr.-Eduard-Martin Award from the University of Saarland in 2002, the National Science Foundation (NSF) CAREER Award in 2003, and the Outstanding Teaching Award from the Department of Electrical Engineering of the University of Washington in 2004. In 2005, he served as advisor to the University of Washington student team that designed a next-generation hydrogen power park and received the honorable mention award from the National Hydrogen Association.